Hindawi
Shock and Vibration
Volume 2022, Article ID 5598689, 11 pages
https://doi.org/10.1155/2022/5598689

Research Article

A Novel Low Stiffness Air Spring Vibration-Isolation Mounting System

Chang-geng Shuai,[1,2] **Bu-yun Li**,[1,2] **Jian-guo Ma**,[1,2] **and Zhao-hao Yang**[1,2]

[1]*Institute of Noise & Vibration, Naval University of Engineering, Wuhan 430033, China*
[2]*National Key Laboratory on Ship Vibration & Noise, Wuhan 430033, China*

Correspondence should be addressed to Jian-guo Ma; mjianguo0722@163.com

Received 1 November 2021; Revised 21 December 2021; Accepted 25 January 2022; Published 21 February 2022

Academic Editor: Zeqi Lu

Quasi-zero-stiffness (QZS) structures offer substantial practical benefits for facilitating the essential support and isolation of vibrational source loads aboard modern marine vessels. In order to design a compact QZS system of high bearing capacity, the article proposes a low stiffness air spring (LSAS) vibration-isolation mounting system composed of both vertical and lateral air springs. The vertical air springs support the load and isolate vibrations in the vertical direction, while the lateral air springs support the load and isolate transversal vibrations. Theoretical analyses based on a simple two-dimensional, single degree of freedom model demonstrate that the proposed novel LSAS design decreases the degree of stiffness in the support structure that would otherwise be induced by introducing lateral air springs and accordingly increases the vibration isolation effect. Moreover, optimization of the air spring parameters enables the lateral air springs to provide negative stiffness and thereby realize QZS characteristics. Experimental testing based on prototypes of a standard air spring mounting system and the proposed LSAS mounting system demonstrates that the stiffness of the proposed system is about 1/5 that of the standard system. Accordingly, the proposed structure design successfully alleviates the undesirable influence of lateral air springs on the stiffness of the mounting system.

1. Introduction

Vibration control is an essential operation in modern marine vessels for supporting numerous factors, such as the acoustic stealth of vessels, the living comfort of passengers, the working performance of on-board precision instruments, and the service life of the equipment. Vibration isolation has been the most widely adopted method for this purpose [1]. The general aim of vibration isolation systems is to reduce the level of vibrations transmitted to primary ship structures from vibration sources, such as marine propulsion units (MPUs), generators, ventilation units, and pumps. The most common vibration isolation systems employed in marine vessels include single-stage vibration isolation systems, double-stage vibration isolation systems, and floating raft vibration isolation systems [2].

The primary components increasingly employed in the above-discussed vibration isolation systems are air springs. Accordingly, the design of high-performance air springs has been the subject of intense interest for developing advanced vibration isolation systems. The development of air springs has greatly contributed to the effective isolation of vibrations arising from large-scale on-board equipment. These efforts have been further supported by the development of a new type of air spring with numerous advantages, such as high working pressure, large load capacity, compact structure, and low natural oscillation frequency [3–5].

In addition to designing advanced air springs, efforts have been applied to developing more advanced vibration isolation systems, such as quasi-zero-stiffness (QZS) structures. A QZS structure has the advantage of high-static-low-dynamic stiffness, which can provide enhanced vibration isolation performance relative to linear systems. The important research part of the QZS structure is to use the benefit of nonlinearity [6]. A typical approach applied for designing a QZS structure involves the use of oblique

springs. For example, Carrella et al. [7] proposed a simple QZS isolator model comprising two oblique springs in parallel with a vertical spring and studied the restoring force and force transmissibility characteristics of the system. Subsequently, a more in-depth dynamic analysis of this nonlinear mechanism with three springs was conducted [8, 9]. On this basis, researchers have used a linkage and two noninclined springs to realize QZS characteristics under small deflection [10], while large deflection conditions have been accommodated using a combination of two inclined links, one noninclined spring, and two orientating springs [11]. Another typical approach applied for designing QZS isolators involves using X-shaped, bioinspired, and ring shape structures. For example, Sun and Jing [12] evaluated the vibration isolation performance of X-shaped isolators. Other studies proposed bioinspired X-shaped structures appropriate for different engineering practices [13–15]. Lu et al. [16] investigated the dynamical characteristics of a circular ring shape isolator, and the results demonstrated that this shape exhibited a nonlinear stiffness that enhanced its vibration isolation efficiency. Magnetic springs have also been used to design nonlinear QZS vibration isolators. For example, Xu et al. [17] applied magnetic springs to design a nonlinear vibration isolator for low-frequency applications. Wu et al. [18] proposed a vibration isolator that combines a coil spring in parallel with a magnetic spring with negative stiffness. Zhang et al. [19] utilized the variable reluctance stress of a magnetic spring to generate a negative stiffness. Yuan et al. [20] designed an electromagnetic spring with negative stiffness over a long stroke by combining three toroidal coils arranged coaxially with a ring magnet. Finally, special materials have been employed to design nonlinear QZS vibration isolators. For example, Lu et al. [21] used a bistable carbon fiber-metal composite plate for realizing low-frequency vibration isolation. Li et al. [22] designed a mechanical molecular spring isolator to realize high-static-low-dynamic stiffness.

The above discussion demonstrates that QZS structures offer substantial practical benefits for providing excellent low-frequency vibration isolation performance. The vibration isolation system of vessels should have a compact structure and large bearing capacity, which the current air spring vibration isolation system can satisfy. Inspired by the nonlinear structures discussed above, this article proposes a novel low stiffness air spring (LSAS) vibration-isolation mounting system based on a standard air spring vibration isolation system to further improve the vibration isolation ability. The LSAS system is composed of vertical and lateral air springs that, respectively, support the weight of large-scale loads in the vertical and lateral directions while also isolating the respective vibrations in those directions. The proposed LSAS mounting structure is modeled as a simple two-dimensional (2D), single degree of freedom system with displacements limited to the vertical direction. While displacements in the horizontal direction can certainly affect the vibration transmissibility of the structure, the applied simplifications facilitate detailed theoretical analyses for determining the optimal air spring parameters that enable the lateral air springs to provide negative stiffness to the system and thereby realize QZS characteristics. Therefore, the simplifications are quite useful. Finally, prototypes of a standard air spring mounting system and the proposed LSAS mounting system are constructed, and experimental testing demonstrates that the vertical stiffness of the proposed system is about 1/5 that of the standard system. Accordingly, the proposed structure design successfully alleviates the undesirable influence of lateral air springs on the stiffness of the mounting system.

2. Standard Air Spring Vibration-Isolation Mounting Systems

The theoretical analysis is based on the standard three-dimensional (3D) air spring mounting system schematically illustrated in Figure 1. The model is composed of a mass (C), six vertical air springs (A) between C and the floor boundary, and six lateral air springs (B) between C and the wall boundaries. It should be noted that the number of vertical and lateral air springs employed depends entirely on the actual setting and may therefore vary considerably.

Analysis of the mounting system is greatly simplified by adopting the 2D model illustrated in Figure 2(a), along with the corresponding free body diagram given in Figure 2(b). In addition, we assume that no displacements occur in the horizontal direction. Therefore, all forces in the y-direction arising from the lateral air springs are always equal and opposite. Accordingly, the 2D standard air spring mounting system can be viewed as a simple single degree of freedom vibration isolation system.

Under the assumption of small displacements x, the vertical restoring force (F_{0x}) of the single vertical air spring and the transversal restoring force (F_{1x}) of a single lateral air spring can be approximately given as the following first-order functions of deformation:

$$F_{0x} = k_{xx}x + F_{vv0}. \tag{1}$$

$$F_{1x} = k_{yy}x. \tag{2}$$

Here, k_{xx} and k_{yy} are the vertical stiffness and transversal stiffness coefficients of the air springs, respectively, and F_{vv0} is the initial vertical force associated with the weight of C. According to (1) and (2), the total restoring force and stiffness of the standard air spring mounting system illustrated in Figure 2(b) can be, respectively, given as follows:

$$\begin{aligned} F_{r-s} &= F_{0x} + 2F_{1x} = k_{xx}x + 2k_{yy}x, \\ k_{r-s} &= k_{xx} + 2k_{yy}. \end{aligned} \tag{3}$$

Similarly, the force transmissibility of the standard air spring mounting system can be given as follows:

$$T_s = \sqrt{\frac{k_{r-s} + 4\xi^2\Omega^2 k_{vv}}{k_{r-s}\left(1 - \Omega^2 k_{xx}/k_{r-s}\right)^2 + 4\xi^2\Omega^2 k_{xx}}}. \tag{4}$$

Here, Ω represents the excitation frequency and ξ is the damping coefficient of the system. Finally, the force

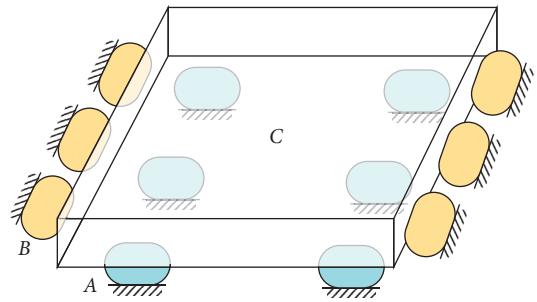

FIGURE 1: Three-dimensional (3D) schematic illustrating a representative standard air spring mounting system: (A) vertical air springs; (B) lateral air springs; (C) supported mass. Please note that the number of air springs applied depends entirely on the actual setting.

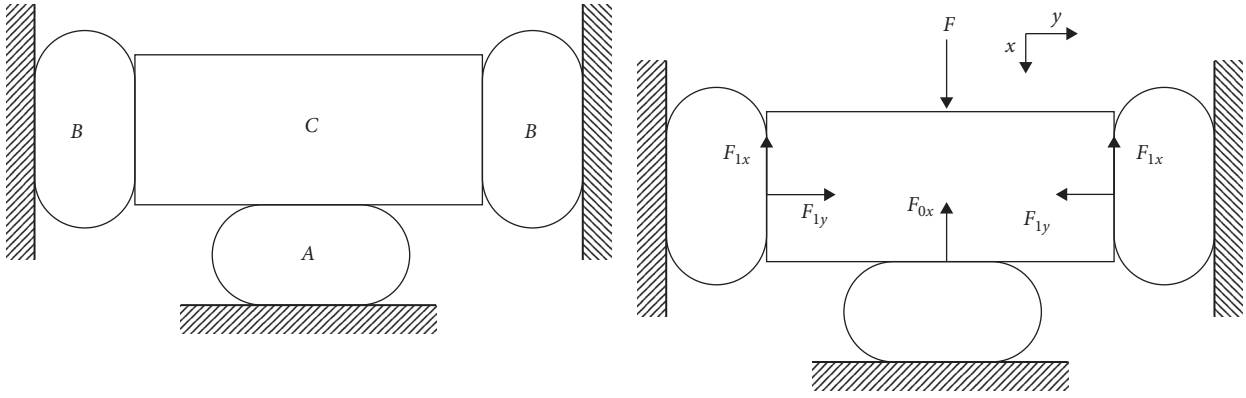

FIGURE 2: The simplified standard air spring mounting system: (a) two-dimensional (2D) schematic and (b) free body diagram.

transmissibility of a single vertical standard air spring mounting structure can be given as follows [23]:

$$T_a = \sqrt{\frac{1 + 4\xi^2\Omega^2}{\left(1 - \Omega^2\right)^2 + 4\xi^2\Omega^2}}. \quad (5)$$

The values of T_s and T_a are plotted in Figure 3 as a function of excitation frequency Ω applied in the vertical direction for all air springs with uniform internal pressures of 1.7 MPa. The relationships between the internal air pressure and the stiffness coefficients of the air springs are presented in Table 1. These results demonstrate that the introduction of lateral air springs makes the natural oscillation frequency of the standard system (Ω_2) 2 times greater than that of the single vertical air spring structure (Ω_1) and accordingly reduces the vibration isolation effect of the system.

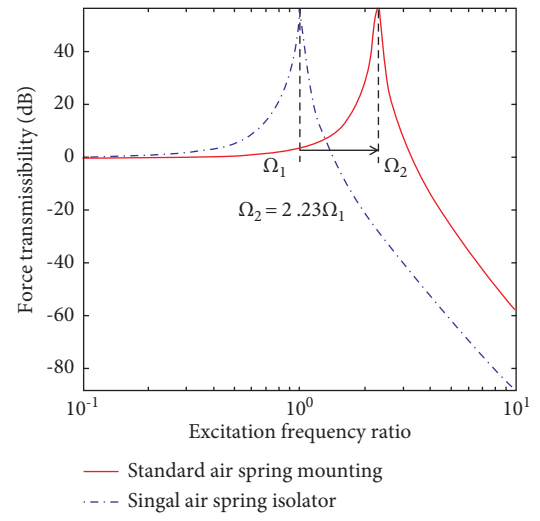

FIGURE 3: Comparison of force transmissibility values obtained by the standard air spring mounting system and a single vertical air spring mounting structure as a function of the excitation frequency.

3. Low Stiffness Air Spring Mounting Design

3.1. Model. The proposed LSAS mounting system is illustrated schematically in Figure 4. The primary difference between this model and the standard model in Figure 2(a) is that connectors are rigidly connected to the cover plates of the lateral air springs, flexibly connected by universal joints, and then rigidly connected to C to address the undesirable effect of the lateral air springs on the vibration isolation system. Here, Figure 4 represents a static equilibrium condition, where the vertical spring supports the load of the mass, the universal joints are in a nonrotated state, and the connectors lie in the horizontal direction. Accordingly, it is

Table 1: Relationships between the internal air pressure of the air spring and the values of the stiffness coefficients used in the mathematical models, and the weight of a supported mass (F_{vv0}).

Pressure (MPa)	k_{xx} (kN·mm^{-1})	k_{yy} (kN·mm^{-1})	$k_{\theta\theta}$ (kN·mmrad^{-1})	F_{vv0} (kN)	μ_2
1.3	1.8120	4.1746	3500.2	18.1564	2.3
1.5	1.9805	4.3376	3998.4	20.9673	2.2
1.7	2.1292	4.4395	4512.5	24.2636	2.1
1.9	2.2845	4.5137	5001.1	29.9652	2.0
2.1	2.3935	4.5539	5101.3	29.8726	2.0

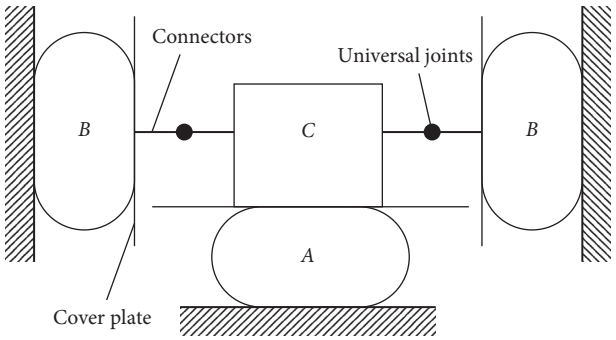

Figure 4: 2D schematic of the proposed low stiffness air spring (LSAS) mounting system at equilibrium.

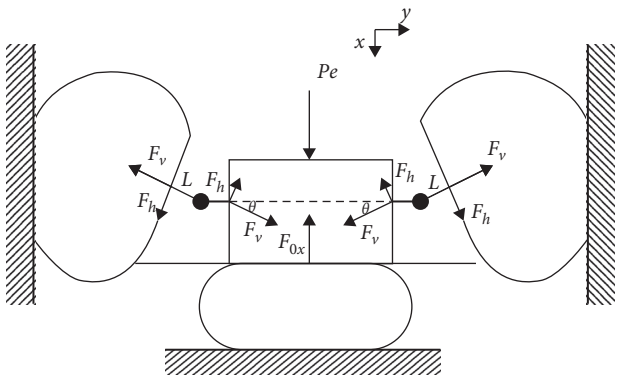

Figure 5: Free body diagram under a non-equilibrium condition.

assumed that the initial installation height is equivalent for both lateral air springs.

3.2. Static Analysis. A nonequilibrium free body diagram corresponding to the schematic illustrated in Figure 4 is given in Figure 5. Here, only the universal joints and lateral air springs are able to rotate, while all other components remain rigidly connected. Therefore, the length of the connectors between the universal joints and the supported mass can be neglected in the analysis because these are merely integral parts of the supported mass. Therefore, the rotation of the lateral air springs is accommodated by their irregular deformation along the cover plates. As such, the supported mass is subjected to a static force P_e composed of F_{0x} and other components of force in the vertical x-direction arising from the linkage between the lateral air springs and C. Again, we assume that no displacements occur in the horizontal direction, and all forces in the horizontal y-direction arising from the lateral air springs are always equal and opposite. Therefore, the vertical air spring deforms only in the x-direction and supports the mass.

We first consider the behavior of the lateral springs in isolation from the vertical air spring. This decoupling of the system is acceptable under the assumption that no displacements occur in the horizontal direction. Therefore, the vertical forces of the vertical air spring and lateral air springs on the supported mass are merely additive. Here, the restoring forces of a single lateral air spring perpendicular to the cover plates (F_v) and along the cover plates (F_h), as well as the torsional moment (M), can be defined according to displacements dx and dy as follows:

$$\begin{aligned} F_v &= -k_{xx}dx + F_{v0}, \\ F_h &= k_{yy}dy, \\ M &= k_{\theta\theta}\theta. \end{aligned} \tag{6}$$

Here, k_{xx}, k_{yy}, and $k_{\theta\theta}$ are the vertical, horizontal, and torsional stiffness coefficients of the lateral air springs, respectively.

The relationships between dx, dy, and θ under deformations in a lateral air spring are illustrated in Figure 6, where Point A and Point B represent the positions of the universal joint in equilibrium and under deformation associated with a vertical displacement x, respectively. Under deformation, the cover plate of the lateral air spring has rotated by an angle θ. For clarification, we also assume that Point A′ also exists that is associated with the same rotation angle θ. Therefore, the relationship between dx, dy, and x can be obtained based on the length L of the connector as follows:

$$\begin{aligned} \frac{\mathrm{d}y}{\cos\theta} + L\tan\theta &= x, \\ b &= \mathrm{d}y\tan\theta, \\ a &= \frac{L}{\cos\theta} - L. \end{aligned} \tag{7}$$

These relationships yield the following two expressions that can be employed to solve dx and dy:

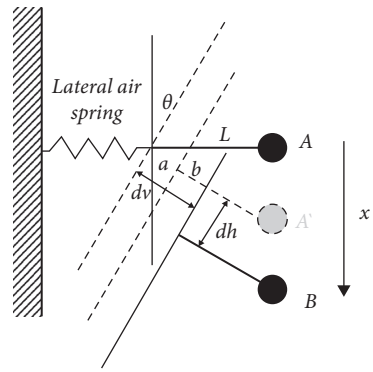

Figure 6: Schematic analysis of lateral air spring deformations.

$$\begin{aligned} \mathrm{d}x &= \mathrm{d}y\ \tan\ \theta + \frac{L}{\cos\ \theta} - L, \\ \mathrm{d}y &= (x - L\ \tan\ \theta)\cos\ \theta. \end{aligned} \tag{8}$$

To facilitate the solution of θ, we adopt the following moment balance analysis of the connector:

$$M = F_h L = k_{\theta\theta}\theta. \tag{9}$$

Accordingly, the total restoring force of the two lateral air springs in the x-direction is defined as follows:

$$F_{r-lateral} = 2\left(F_h \cos\ \theta - F_v \sin\ \theta\right). \tag{10}$$

This expression is simplified by applying the following third-order Taylor series expansion of (10) at $x = 0$ [24]:

$$F_{\mathrm{app},r-\mathrm{lateral}} = \frac{2\left(-F_{v0}Lk_{yy} + k_{yy}k_{\theta\theta}\right)x}{L^2k_{yy} + k_{\theta\theta}} + \frac{\left(F_{v0}L^3k_{yy}^3 + 3L^4k_{xx}k_{yy}^3 - 2L^4k_{yy}^4 + 6L^2k_{xx}k_{yy}^2k_{\theta\theta} - 6L^2k_{yy}^3k_{\theta\theta}\right)x^3}{3\left(L^2k_{yy} + k_{\theta\theta}\right)^3}. \tag{11}$$

The values of $\mathrm{F_{r-lateral}}$ obtained numerically from (10) and $\mathrm{F_{app,r-lateral}}$ obtained from the analytical approximation in (11) are presented in Figure 7 as functions of displacement in the x-direction. The results demonstrate that the analytical solution of the cubic truncation is closer to the numerical solution than that of the quadratic truncation. Therefore, the applied analytical cubic truncation approximation is more acceptable. The overall stiffness contribution of the dual lateral air spring system can be expressed by the derivative of (11) with respect to x as follows:

$$k_{\mathrm{r-lateral}} = \frac{\partial F_{\mathrm{qpp,r-lateral}}}{\partial x}. \tag{12}$$

The dynamic stiffness coefficient for the lateral air springs under the equilibrium condition illustrated in Figure 4 (i.e., $x = 0$) can be given as follows:

$$k_{r-\mathrm{lateral}\,(x=0)} = \frac{2k_{yy}\left(F_{v0}L - k_{\theta\theta}\right)}{L^2k_{yy} + k_{\theta\theta}}. \tag{13}$$

The equation provides a simple analytical expression for defining the contribution the lateral air springs to the overall stiffness of the LSAS system at equilibrium. As can be seen, $\mathrm{k_{r-lateral(}}_{x=0)} > 0$ when $k_{\theta\theta} > F_{\mathrm{v0}}\mathrm{L}$, such that the lateral air springs increase the stiffness of the system. Meanwhile, $\mathrm{k_{r-lateral\ (}}_{x=0)} = 0$, when $k_{\theta\theta} = F_{\mathrm{v0}}\mathrm{L}$, such that the lateral air springs have no effect on the overall stiffness of the system. However, we also find that $\mathrm{k_{r-lateral(}}_{x=0)} < 0$, when $k_{\theta\theta} < F_{\mathrm{v0}}\mathrm{L}$, which indicates that the lateral air springs introduce a negative stiffness to the LSAS system at equilibrium when the torsional stiffness coefficient falls within this range of values. The effects of these different ranges of $k_{\theta\theta}$ on $k_{\mathrm{r-lateral}(x=0)}$ are demonstrated in Figure 8 for different values of L when $F_{\mathrm{v0}} = 18.1564$ kN and $k_{\mathrm{yy}} = 4.518$ kN/mm. The figure marks the points A, B, and C, where $\mathrm{k_{r-lateral(}}_{x=0)} = 0$ for the three different values of L. As can be seen, the range of $\mathrm{k}_{\theta\theta}$ over which $\mathrm{k_{r-lateral(}}_{x=0)} < 0$ increases significantly with increasing L. However, the space required by the LSAS system also increases with increasing L. Therefore, maintaining a sufficiently small value of $\mathrm{k}_{\theta\theta}$ will provide negative stiffness to the system while minimizing the space the system occupies.

We further note from (13) by setting $L = 0$ that $k_{\mathrm{r-lateral}(x=0)} = 2k_{yy}$ for the standard mounting system illustrated in Figure 2(a). Therefore, we can establish the following performance criteria for the proposed LSAS mounting system:

$$k_{r-\mathrm{lateral}\,(x=0)} < 2k_{yy}. \tag{14}$$

Replacing $k_{r-\mathrm{lateral}(x=0)}$ in (14) with the corresponding expression presented in (13) yields the following condition:

$$Lk_{yy} + F_{v0} > 0. \tag{15}$$

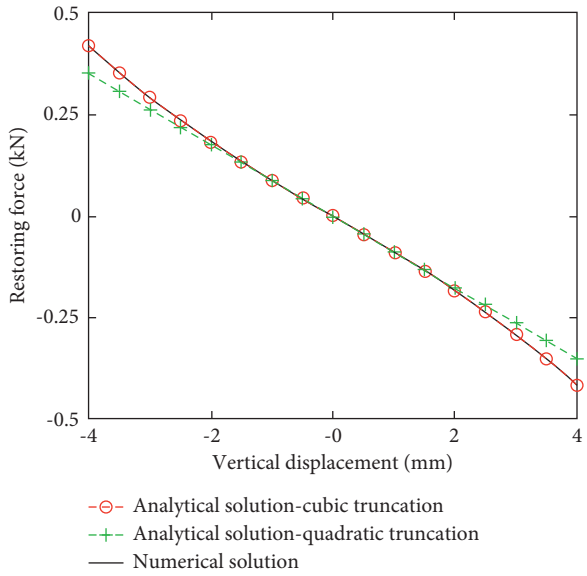

Figure 7: Comparison between the restoring force of a lateral air spring system obtained from the numerical solution and the analytical solution as a function of vertical displacement.

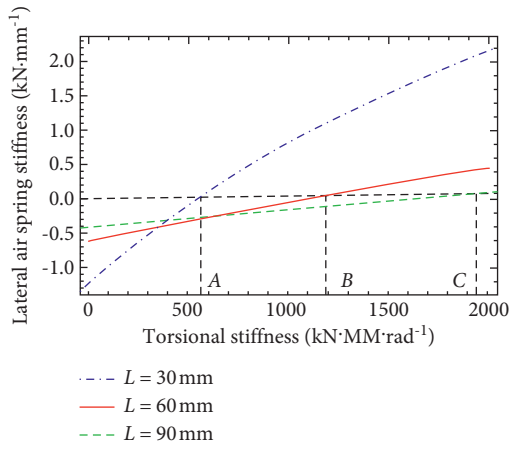

Figure 8: Contribution of the lateral air springs to the vertical stiffness of the LSAS system at equilibrium versus the torsional stiffness $k_{\theta\theta}$ for different connector lengths (L).

This indicates that the proposed LSAS system is guaranteed to at least provide a lower overall stiffness at equilibrium than the standard mounting system, and can potentially function as a QZS system under appropriate conditions involving $k_{\theta\theta}$, F_{v0}, and L.

Then, we extend our analysis of the lateral air springs to include the vertical air spring in the system illustrated in Figure 5. Here, the restoring force of the vertical air spring over small displacements x is

$$F_{0x} = k_{vv}x + F_{vv0}, \tag{16}$$

where k_{vv} is the vertical stiffness of the air spring and F_{vv0} is its initial force applied to the load, which is equal and opposite to the force of the load. Therefore, the total restoring force of the LSAS system is

$$F_{r-LSAS} = F_{0x} + F_{app,r-\text{lateral}} - mg. \tag{17}$$

where m is the mass of the supported load and g is the acceleration due to gravity. Introducing nondimensional parameters $\widehat{F}_{v0} = F_{v0}/k_{xx}L$, $\mu_1 = k_{\theta\theta}/k_{yy}L^2$, $\mu_2 = k_{xx}/k_{yy}$, $\widehat{k}_{r-\text{lateral}} = k_{r-\text{lateral}}/k_{xx}$, $\alpha = k_{vv}/k_{xx}$, $\widehat{x} = x/L$ yields the following dimensionless form of (17):

$$\widehat{F}_{r-LSAS} = \alpha\widehat{x} + \frac{\widehat{F}_{v0}\widehat{x}^3}{3(1+\mu_1)^3} + \frac{\widehat{x}^3}{(1+\mu_1)^3} + \frac{2\widehat{x}^3\mu_1}{(1+\mu_1)^3} - \frac{2\widehat{x}^3}{3\mu_2(1+\mu_1)^3} - \frac{2\widehat{x}^3\mu_1}{\mu_2(1+\mu_1)^3} - \frac{2\widehat{F}_{v0}\widehat{x}}{1+\mu_1} + \frac{2\widehat{x}\mu_1}{\mu_2(1+\mu_1)}. \tag{18}$$

The nondimensional stiffness of the system can be obtained by differentiating (18) with respect to $\widehat{x}$ as follows:

$$\widehat{k}_{r-LSAS} = \alpha + \frac{\widehat{F}_{v0}\widehat{x}^2}{(1+\mu_1)^3} + \frac{3\widehat{x}^2}{(1+\mu_1)^3} + \frac{6\widehat{x}^2\mu_1}{(1+\mu_1)^3} - \frac{2\widehat{x}^2}{\mu_2(1+\mu_1)^3} - \frac{6\widehat{x}^2\mu_1}{\mu_2(1+\mu_1)^3} - \frac{2\widehat{F}_{v0}}{1+\mu_1} + \frac{2\mu_1}{\mu_2(1+\mu_1)}. \tag{19}$$

Finally, the condition of zero stiffness for the LSAS mounting system can be obtained by setting $\widehat{k}_{r-LSAS(\widehat{x}=t0)} = 0$, which yields the following expression:

$$\alpha = -\frac{2\left(\mu_1 - \widehat{F}_{v0}\mu_2\right)}{(1+\mu_1)\mu_2}. \tag{20}$$

Equation (20) provides a simple analytical condition for ensuring that the LSAS system achieves QZS performance. For instance, after carefully designing the lateral air spring to introduce negative stiffness at equilibrium, a QZS state can be ensured to satisfy (14). This example is illustrated by the effects of small dimensionless vertical displacements on $F_{r-\text{LSAS}}$ demonstrated in Figure 9(a) for different values of α when $\mu_1 = 0.03$, $\mu_2 = 0.4$, and the lateral air springs have been designed to introduce negative stiffness. The results demonstrate that the LSAS system behavior can be strongly nonlinear, and a value of $\alpha_{QZS} = 0.175$ provides QZS behavior over a relatively wide region of displacements about the equilibrium point. Therefore, the value of α should be greater than α_{QZS} to avoid negative stiffness near the equilibrium point.

A counterexample was also considered when the lateral air springs have been designed to introduce positive stiffness (i.e., $k_{\theta\theta} > F_{v0}L$). The same conditions employed for Figure 9(a) were employed again with $\alpha_{QZS} = 0.175$, $\mu_2 = 0.4$, and the effects of small dimensionless vertical displacements on $F_{\text{r-LSAS}}$ are demonstrated in Figure 9(b) for different values of μ_1 under the positive stiffness setting. The results demonstrate that the restoring force of the LSAS system behaves linearly under

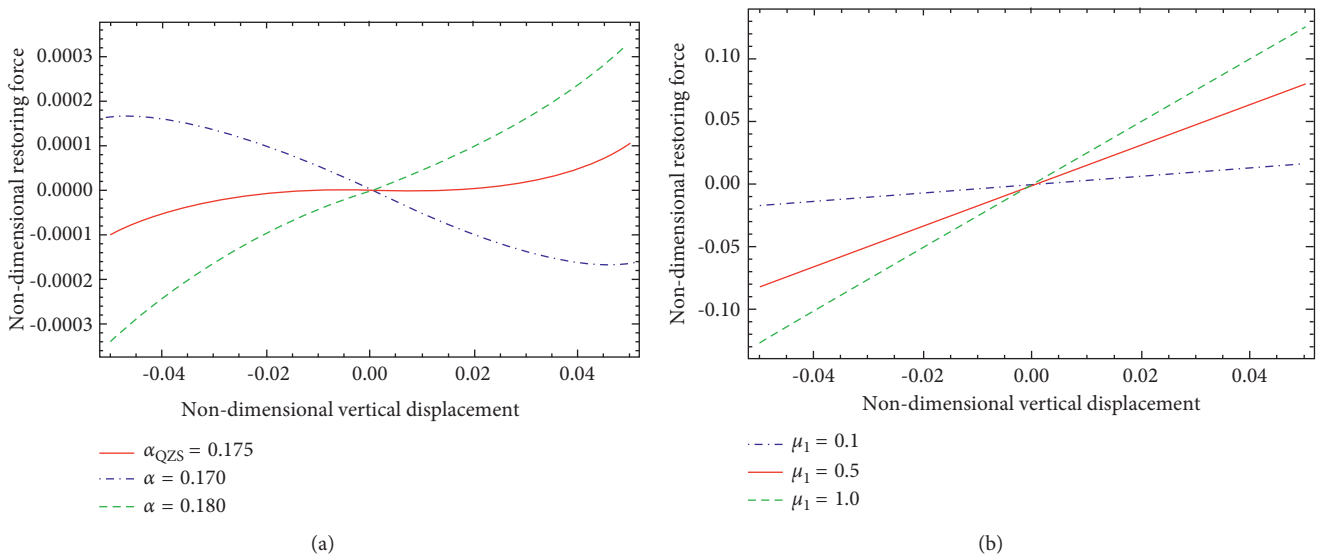

FIGURE 9: Restoring force of the proposed LSAS system as a function of small dimensionless vertical displacements for different values of α: (a) when the lateral air springs are designed to introduce negative stiffness and (b) when the lateral air springs are designed to introduce positive stiffness.

this setting. The observed linearity indicates that the nonlinear components of equation (22) are small when the lateral air springs have been designed to introduce positive stiffness. And as μ_1 decreases, the slope of the force-displacement curve also decreases.

3.3. Dynamic Analysis. It is demonstrated in Section 3.2 that as the lateral air springs provide negative stiffness, the vertical air spring can be adjusted to satisfy the QZS condition. The dynamic equation of the system can be illustrated by the Duffing equation [25]. However, current air springs can only provide positive stiffness for the system. Therefore, we make use of the fact demonstrated above that the nonlinear terms in (18) are small to simplify the analysis by applying a Taylor series expansion.

A first-order Taylor series is defined as follows:

$$f = f(0) + f'(0)\hat{x}. \tag{21}$$

This simple first-order form is acceptable for small displacements about the equilibrium point $\hat{x} = 0$. Accordingly, (18) can be approximated as follows:

$$\hat{F}_{r-app} = \left(\alpha - \frac{2\hat{F}_{v0}}{1+\mu_1} + \frac{2\mu_1}{(1+\mu_1)\mu_2}\right)x. \tag{22}$$

This can be simplified further by setting $\hat{k} = \alpha - 2F_{v0}/1 + \mu_1 + 2\mu_1/(1+\mu_1)\mu_2$. Then, the nondimensional equation of motion for the LSAS system under harmonic excitation is given as follows:

$$\ddot{\hat{x}} + 2\xi\dot{\hat{x}} + \hat{k}\hat{x} = \hat{f}\cos(\Omega_1\tau). \tag{23}$$

Here, ${\omega_0}^2 = k_{xx}/m$, $\tau = \omega_0 t$, $\xi = c/2m\omega_0$, $\Omega_1 = \omega/\omega_0$, and $\hat{f} = f_0/k_{xx}L$. where ω_0 is the fundamental frequency, ω is the excitation frequency, t is time, c is the damping coefficient, and f_0 is the excitation amplitude. Finally, the force transmissibility of the LSAS system can be given as follows:

$$T_{LSAS} = \sqrt{\frac{1 + 4\xi^2\Omega_1^2}{\left(1 - \Omega_1^2\right)^2 + 4\xi^2\Omega_1^2}}. \tag{24}$$

We compare the force transmissibility values obtained for a single vertical air spring ((5)), a standard air spring mounting system ((4)), and the proposed LSAS mounting system ((24)) in Figure 10. These results demonstrate that the decreased vibration isolation effect obtained when adding lateral air springs within the air spring system has been mitigated to a large extent by the proposed LSAS system, where the excitation response of the LSAS system is very similar to the response observed for a single vertical air spring. The results further demonstrate that the vibration isolation effect of the LSAS system increases with decreasing μ_1.

4. Experiments

Four air spring mounting system prototypes were employed for experimental testing. The prototypes are defined as follows:

Prototype I: the proposed LSAS mounting system ($\mu_1 = 0.3$)

Prototype II: the proposed LSAS mounting system ($\mu_1 = 0.03$)

Prototype III: standard system, where the connector and the universal joint assemblies have been removed and the lateral air springs are directly connected to the supported mass

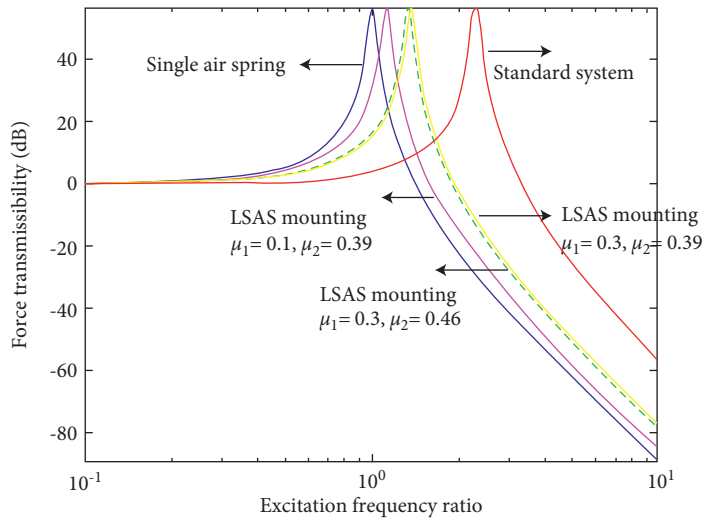

FIGURE 10: Comparison of force transmissibility values obtained by the proposed LSAS mounting system, the standard air spring mounting system, and a single vertical air spring mounting structure as a function of the excitation frequency.

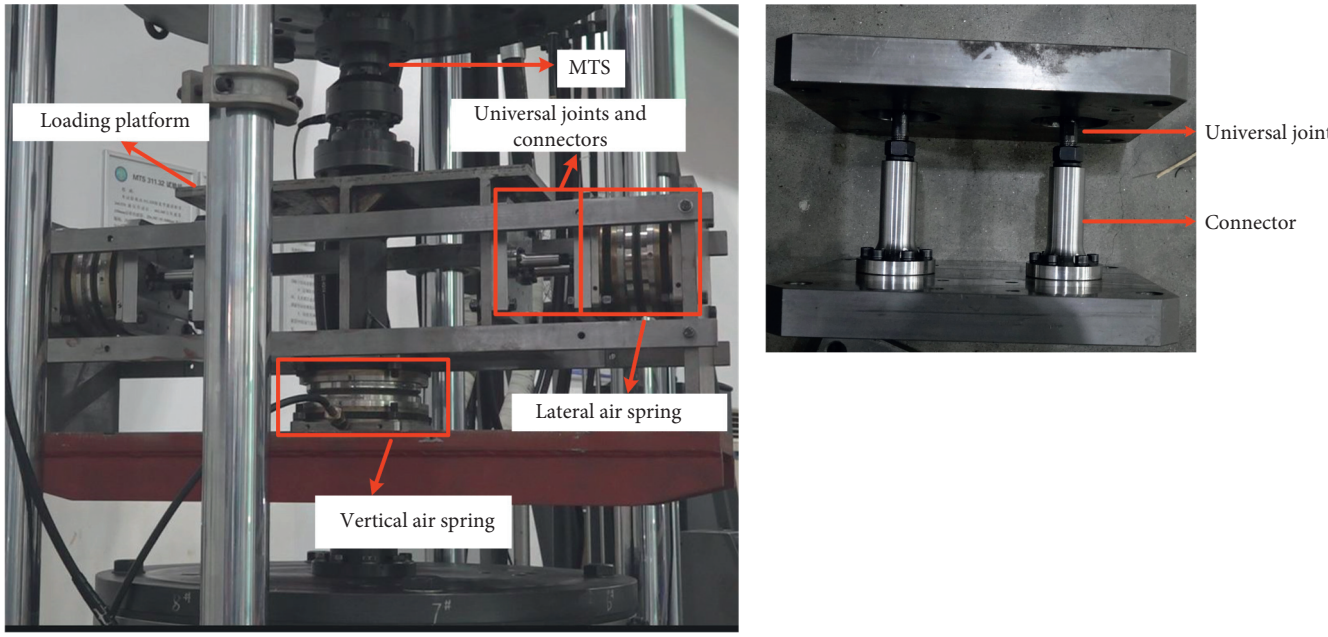

FIGURE 11: Prototype LSAS mounting system: (a) general layout and system components and (b) structure of the connector and universal joint assemblies.

Prototype IV: single vertical air spring, where the lateral air springs and the connector and universal joint assemblies have been removed

Images of the general layout of the test system and the connector and universal joint assemblies are presented in Figures 11(a) and 11(b), respectively. All testing was conducted on an MTS Landmark® 370-50 servohydraulic test system, and the test data were recorded using an MTS software program. The vertical displacement amplitude of the servohydraulic system was set as ±4 mm, and the displacement frequency was set as 1/16 Hz, resulting in a displacement speed of 0.1 mm/s. A uniform test mass of 1000 kg and an internal vertical air spring pressure of 1.7 MPa was employed for all tests. Various internal lateral air spring pressures were employed during testing, including values in the range of 1.3, 1.5, 1.7, 1.9, and 2.1 MPa. As indicated in Table 1, these changes in lateral air spring pressure naturally affected the values of $k_{\theta\theta}$ and $\mu_2 = k_{xx}/k_{yy}$, and the value of the nondimensional parameter $\mu_1 = k_{\theta\theta}/(k_{yy}L^2)$ was fixed at 0.3 or 0.03 by setting the value of L as 60 mm and 165 mm, respectively. However, we further note from Table 1 that these changes in lateral air spring pressure

Table 2: Experimental vertical stiffness results obtained with different lateral air spring pressures P.

P (MPa)	Prototype I (kN·mm^{-1})	Prototype II (kN·mm^{-1})	Prototype III (kN·mm^{-1})	Prototype IV (kN·mm^{-1})
1.3	3.117	2.194	10.50	2.047
1.5	3.201	2.246	10.73	2.047
1.7	3.290	2.268	10.96	2.047
1.9	3.367	2.290	11.18	2.047
2.1	3.466	2.313	11.43	2.047

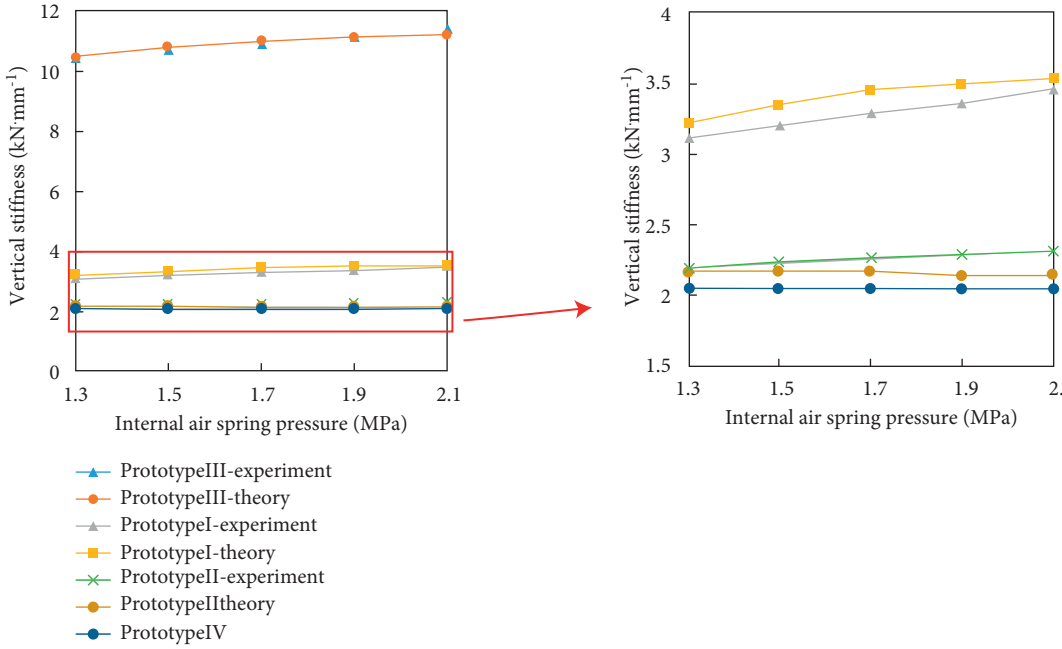

Figure 12: Comparison of experimental and theoretical results obtained for the vertical stiffness of the various vibration isolation mounting systems at the equilibrium point as a function of the internal lateral air spring pressure P.

had little effect on the value of the nondimensional parameter μ_2.

The experimental vertical stiffness results obtained for the four prototype systems with different lateral air spring pressures P are listed in Table 2. Naturally, the vertical stiffness results obtained for prototype IV were constant because the system included no lateral air springs. However, all other prototype systems exhibited an increasing vertical stiffness with increasing P. Moreover, these vertical stiffness values were greater than that of prototype IV under all internal pressures considered, demonstrating that the introduction of lateral air springs increased the vertical stiffness of the mounting systems. However, the fact that the vertical stiffness of prototype II was uniformly less than that of prototype I for all values of P considered confirms the positive effect of applying a decreasing value of μ_1, as demonstrated by the theoretical analysis. Moreover, the vertical stiffness of prototype II was approximately 1/5 of that obtained by prototype III for all values of P considered, which again clearly confirms the results of theoretical analysis. Finally, the experimental results demonstrate that the vertical stiffness of prototype II was only about 7% greater than that of prototype IV at $P = 1.3$ MPa, which confirms the results of theoretical analysis demonstrating that the proposed connector and universal joint assemblies mitigate the increased stiffness arising from the incorporation of lateral air springs.

The validity of the theoretical analysis is further demonstrated in Figure 12 by comparing the experimental vertical stiffness results with the corresponding theoretical results obtained at the equilibrium point. We note that the agreement between the observed dependencies on P is excellent, which supports the validity of both the theoretical analyses and the experimental results.

5. Conclusion

The present work proposed a novel LSAS vibration-isolation mounting system composed of both vertical and lateral air springs with connectors and universal joints. Theoretical analyses based on a simple 2D, single degree of freedom model demonstrated that the proposed novel LSAS design decreases the degree of stiffness in the support structure that would otherwise be induced by introducing lateral air springs and accordingly increases the vibration isolation effect. Moreover, optimization of the air spring parameters enables the lateral air springs to provide negative stiffness, thereby realizing QZS characteristics. Finally, the results of

experiments employing prototypes of a standard air spring mounting system and the proposed LSAS mounting system demonstrated that the vertical stiffness of the proposed system is about 1/5 that of the standard system. Accordingly, the proposed structure design successfully alleviates the undesirable influence of lateral air springs on the stiffness of the mounting system. We must also note the limitations of the present study associated with an omission of lateral displacements. While displacements in the horizontal direction can certainly affect the vibration transmissibility of the structure, the simplified 2D, single degree of freedom model applied in the present work facilitated detailed theoretical analyses for determining the optimal air spring parameters that enable the lateral air springs to provide negative stiffness to the system and thereby realize QZS characteristics. The clarity obtained by these simplifications was extremely beneficial for illustrating the specific factors affecting the QZS characteristics of the proposed mounting structure. These simplifications also provided a clear means of verifying the theoretical analyses via experimental testing and can be applied in later work considering a more rigorously complete model for redesigning the lateral air springs to provide negative stiffness and thereby realize QZS characteristics.

Data Availability

The experimental data used to support the findings of this study are available from the corresponding author upon request.

Conflicts of Interest

The authors declare no potential conflicts of interest with respect to the research, authorship, and/or publication of this article.

Acknowledgments

The authors gratefully acknowledge support for this work by the National Key Research and Development Program of China (Grant no. HJ2019C020499).

References

[1] C. Q. Howard, "Recent developments in submarine vibration isolation and noise control," in *Submarine Science Technology and Engineering Conference*, M. Sander, Ed., pp. 283–290, Engineers Australia, Adelaide, Australia, 2011.

[2] L. He and W. Xu, "Naval vessel machinery mounting technology and its recent advances," *Acta Acustica*, vol. 38, no. 2, pp. 128–136, 2013.

[3] L. He, W. Xu, W. Bu, and L. Shi, "Dynamic analysis and design of air spring mounting system for marine propulsion system," *Journal of Sound and Vibration*, vol. 333, no. 20, pp. 4912–4929, 2014.

[4] Z. Q. Lv, L. He, and C. G. Shuai, "Optimization of natural frequencies of large-scale two-stage raft system," *Journal of Physics Conference*, vol. 744, Article ID 012180, 2016.

[5] Y. Li, L. He, C.-g. Shuai, and C.-y. Wang, "Improved hybrid isolator with maglev actuator integrated in air spring for active-passive isolation of ship machinery vibration," *Journal of Sound and Vibration*, vol. 407, pp. 226–239, 2017.

[6] S. M. M. Mofifidian and H. Bardaweel, "Displacement transmissibility evaluation of vibration isolation system employing nonlinear-damping and nonlinear-stiffness elements," *Journal of Vibration and Control*, vol. 24, no. 18, pp. 4247–4259, 2018.

[7] A. Carrella, M. J. Brennan, and T. P. Waters, "Static analysis of a passive vibration isolator with quasi-zero-stiffness characteristic," *Journal Of Sound And Vibration*, vol. 301, no. 3-5, pp. 678–689, 2007.

[8] I. Kovacic, M. J. Brennan, and T. P. Waters, "A study of a nonlinear vibration isolator with a quasi-zero stiffness characteristic," *Journal of Sound and Vibration*, vol. 315, no. 3, pp. 700–711, 2008.

[9] A. Carrella, M. J. Brennan, I. Kovacic, and T. P. Waters, "On the force transmissibility of a vibration isolator with quasi-zero-stiffness," *Journal of Sound and Vibration*, vol. 322, no. 4-5, pp. 707–717, 2009.

[10] G. Gatti, A. D. Shaw, P. J. P. Gonçalves, and M. J. Brennan, "On the detailed design of a quasi-zero stiffness device to assist in the realisation of a translational Lanchester damper," *Mechanical Systems and Signal Processing*, vol. 164, Article ID 108258, 2022.

[11] A. D. Shaw, G. Gatti, P. J. P. Gonçalves, B. Tang, and M. J. Brennan, "Design and test of an adjustable quasi-zero stiffness device and its use to suspend masses on a multi-modal structure," *Mechanical Systems and Signal Processing*, vol. 152, Article ID 107354, 2021.

[12] X. Sun and X. Jing, "A nonlinear vibration isolator achieving high-static-low-dynamic stiffness and tunable anti-resonance frequency band," *Mechanical Systems and Signal Processing*, vol. 80, pp. 166–188, 2016.

[13] G. Q. Jiang, X. J. Jing, and Y. Q. Guo, "A novel bio-inspired multi-joint anti-vibration structure and its nonlinear HSLDS properties," *Mechanical Systems and Signal Processing*, vol. 138, Article ID 106552, 2020.

[14] X. Jing, L. Zhang, X. Feng, B. Sun, and Q. Li, "A novel bio-inspired anti-vibration structure for operating hand-held jackhammers," *Mechanical Systems and Signal Processing*, vol. 118, pp. 317–339, 2019.

[15] H. Dai, X. Jing, Y. Wang, X. Yue, and J. Yuan, "Post-capture vibration suppression of spacecraft via a bio-inspired isolation system," *Mechanical Systems and Signal Processing*, vol. 105, pp. 214–240, 2018.

[16] Z. Q. Lu, D. H. Gu, H. Ding, W. Lacarbonara, and L. Q. Chen, "Nonlinear vibration isolation via a circular ring," *Mechanical Systems and Signal Processing*, vol. 163, Article ID 106490, 2020.

[17] D. Xu, Q. Yu, J. Zhou, and S. R. Bishop, "Theoretical and experimental analyses of a nonlinear magnetic vibration isolator with quasi-zero-stiffness characteristic," *Journal of Sound and Vibration*, vol. 332, no. 14, pp. 3377–3389, 2013.

[18] W. Wu, X. Chen, and Y. Shan, "Analysis and experiment of a vibration isolator using a novel magnetic spring with negative stiffness," *Journal of Sound and Vibration*, vol. 333, no. 13, pp. 2958–2970, 2014.

[19] F. Zhang, M. L. Xu, S. B. Shao, and S. L. Xie, "A new high-static-low-dynamic stiffness vibration isolator based on magnetic negative stiffness mechanism employing variable reluctance stress," *Journal of Sound and Vibration*, vol. 476, Article ID 115322, 2020.

[20] S. J. Yuan, Y. Sun, and J. L. Zhao, "A tunable quasi-zero stiffness isolator based on a linear electromagnetic spring,"

Journal of Sound and Vibration, vol. 482, Article ID 115449, 2020.

[21] Z. Q. Lu, T. J. Yang, and M. J. Brennan, "Experimental investigation of a two-stage nonlinear vibration isolation system with high-static-low-dynamic stiffness," *Journal of Applied Mechanics*, vol. 84, no. 2, Article ID 021001, 2017.

[22] Z. Y. Li, Q. Chen, F. S. Gu, and A. Ball, "Modeling a mechanical molecular spring isolator with high-static-low-dynamic-stiffness properties," " *Shock and Vibration*, vol. 2020, Article ID 8853936, 2020.

[23] C. M. Harris and A. G. Piersol, *Shock and Vibrations Handbook*, McGraw-Hill, New York, NY, USA, 2010.

[24] W. C. Ray, *Advanced Engineering Mathematics*, McGraw-Hill, New York, NY, USA, 1960.

[25] Y. Li and D. Xu, "Force transmissibility of floating raft systems with quasi-zero-stiffness isolators," *Journal of Vibration and Control*, vol. 24, pp. 3608–3616, 2016.